Molecular Based Mathematical Biology
Research Article • DOI: 10.2478/mlbmb-2013-0005 • MBMB • 2012 • 90-108

VERSITA

Parallel Adaptive Finite Element Algorithms for Solving the Coupled Electro-diffusion Equations

Abstract

In this paper we present parallel adaptive finite element algorithms for solving the 3D electro-diffusion equations such as the Poisson-Nernst-Planck equations and the size-modified Poisson-Nernst-Planck equations in simulations of biomolecular systems in ionic liquid. A set of transformation methods based on the generalized Slotboom variables is used to solve the coupled equations. Calculations of the diffusion-reaction rate coefficients, electrostatic potential and ion concentrations for various systems verify the method's validity and stability. The iterations between the Poisson equation and the Nernst-Planck equations in the primitive method and in the transformation method are compared to illustrate how the new method accelerates the convergence of the solution. To speed up the convergence, we introduce the DIIS (direct inversion of the iterative subspace) method including Simple Mixing and Anderson Mixing as under-relaxation techniques, the effectiveness of which on acceleration is shown by numerical tests. It is worth noting that the primitive method fails to solve the size-modified Poisson-Nernst-Planck equations for real protein systems but the transformation method succeeds in the simulations of the ACh-AChE reaction system and the DNA fragment. To improve the accuracy of the solution, we introduce high order elements and mesh adaptation based on an *a posteriori* error estimator. Numerical results indicate that our mesh adaptation process leads to quasi-optimal convergence. We implement our algorithms using the parallel adaptive finite element package PHG [53] and high parallel efficiency is obtained.

Keywords

Poisson-Nernst-Planck equations • Adaptive Finite Element Method • DIIS • Parallel Processing • Slotboom variables • PHG

MSC: 35Q92, 35Q70

Yan Xie*, Jie Cheng†, Benzhuo Lu‡, Linbo Zhang§

State Key Laboratory of Scientific and Engineering Computing, Institute of Computational Mathematics and Scientific/Engineering Computing, Academy of Mathematics and Systems Science, Chinese Academy of Sciences, Beijing 100190, China

Received 2012-09-25
Accepted 2013-03-19

1. Introduction

Electrostatic potential and ion distribution around molecular species are essential for describing electro-diffusion, a rate-limiting step in numerous biological processes, such as ligand-enzyme binding and protein-protein diffusive encounter. If the particle-particle correlations of the diffusing species are neglected, the Poisson-Nernst-Planck equations (PNPEs)

* *E-mail: xieyan@lsec.cc.ac.cn*
† *E-mail: chengjie@lsec.cc.ac.cn*
‡ *E-mail: bzlu@lsec.cc.ac.cn (Corresponding author)*
§ *E-mail: zlb@lsec.cc.ac.cn (Corresponding author)*

are a proper continuum model for describing the electro-diffusion process of ions via coupling electrostatic potential to ionic diffusion [33]. PNPEs are used to simulate ion channels [44,26,31,21,5,7,17,54] and ion migrations [29]. In this paper we adopt the Poisson-Nernst-Planck equations and the size-modified PNP equations to describe the electro-diffusion-reaction of mobile ions and charged ligands, all modeled as diffusive particles with vanishing size and finite size effects respectively, in the solvated biomolecular system. Here the electrostatic potential is induced by the mobile ions, charged ligands and the fixed charges carried by biomolecules.

Figure 1 illustrates biomolecular solution system occupying a domain Ω with a smooth boundary Γ_s. The domain Ω_s denotes the solvent region that contains several diffusing species while the domain Ω_m denotes the macro-biomolecule(s) region. Here, $\Omega = \Omega_s \cup \Omega_m$. Γ_m denotes the boundary of Ω_m. A small patch Γ_a ($\Gamma_a \in \Gamma_m$) around the active site is set to a zero Dirichlet boundary condition to model the chemical reaction.

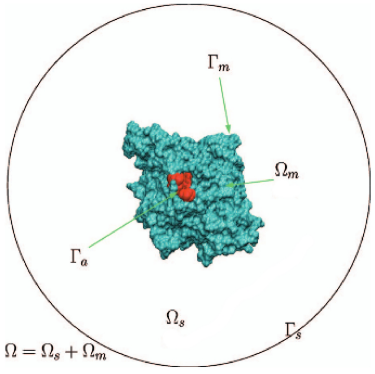

Fig 1. Schematic illustration of the computational domain modeling electro-diffusion reaction processes in the biomolecular solution system.

The Poisson-Nernst-Planck equations (PNPEs) describe the coupling of potential field, density distribution and diffusion processes as follows:

$$\frac{\partial p_i}{\partial t} = \nabla \cdot \{D_i(\nabla p_i + \beta \nabla(q_i \phi) p_i)\}, \text{ in } \Omega_s,\ i = 1, \ldots, K. \tag{1}$$

$$-\nabla \cdot \epsilon \nabla \phi = \rho^f + \lambda \sum_{i=1}^{K} q_i p_i, \text{ in } \Omega. \tag{2}$$

where p_i and ϕ are unknowns. p_i is the density distribution function of the diffusing particles of the ith species with diffusion constant D_i. ϕ is the electrostatic potential that imposes driving forces on the diffusing particles. The other variables are given as constants. $\lambda = 0$ in Ω_m and $\lambda = 1$ in Ω_s, K is the number of species considered, $\beta = 1/k_B T$ is the inverse Boltzmann energy, k_B is the Boltzmann constant, T is the temperature and ϵ is the dielectric coefficient. $q_i = z_i e_c$ is the charge of each particle of the ith species, e_c is the elementary charge. The permanent (fixed) charge distribution $\rho^f(x) = \sum_j q_j \delta(x - x_j)$ is an ensemble of singular charges q_j located at x_j inside biomolecules. See [23] for details about units and physical constants.

Both the potential and ion concentration gradients contribute to the movement of ions. Ions interact with the atomic charges in the protein and all the other mobile ions in solvent. The PNP model is able to generate a self-consistent electrostatic potential and the non-equilibrium densities. In this paper, we focus on the steady-state diffusion system, i.e. $\frac{\partial p_i}{\partial t} = 0$.

PNPEs are also a proper model for semiconductor device simulations [38,20,2,15,14], for instance, in calculating the $I-V$ characteristics or studying the process of ion transport. Numerical PNPEs solvers have been developed for both simple one-dimensional phenomenological models [12,6,18] and complex 3D models for ion channel permeations [5,47,26]. It is known that the Nonlinear Poisson Boltzmann equation [43,39,32] is a special case of PNPEs at equilibrium in which the ion concentrations follow Boltzmann distributions. Therefore, the PB results are consistent with PNP solution under certain conditions [33]. A variety of numerical methods have been applied to solve PBE as well as PNPEs including finite difference method [30,51,55,54], finite element method (FEM) [40,34,33] and hybrid method [4,36]. In this paper, we

continue to use FEM for solving PNPEs because it is flexible in dealing with irregular shapes in surface biomolecular systems and higher order approximations can be easily obtained by increasing the finite element order.

During past several years, there have been enormous strides in numerical studies of PNP theory. From the point of view of finite element computing, some difficulties in FEM PNP solution have been overcome. The first among these is mesh generation that is fundamental as discretization of computing regions. So far, softwares and packages such as Tetgen [48], TMSmesh [8], ISO2Mesh [19] and TransforMesh [52] are used to generate high resolution meshes. Secondly, open-source finite element computing softwares such as PHG [53] and FETK [24] are publicly available and are successfully used in our work to solve PNP equations. However, there are still problems confronting the finite element computing of PNP models, especially in the area of biomolecular simulation. Firstly, qualified, stable and efficient molecular surface/volume meshing appears to be necessitated by recent developments for realistic mathematical modeling and numerical simulation of biomolecules, especially in implicit solvent modeling. Secondly, in the solution of the PNP equations system, direct iterative approaches between coupling equations sometimes fail to converge or converge at a slow speed, therefore relaxation or other techniques need to be introduced to speed up convergence. For the more complicated size-modified PNP equations, we found our previous primitive relaxation iterative approaches fail to converge when applied to protein and DNA systems other than the very simple sphere cavity model [35]. The size-modified PNPEs (SMPNP) are written as

$$\frac{\partial p_i}{\partial t} = \nabla \cdot D^i \left(\nabla p_i + \frac{k_i p_i}{1 - \sum_l a_l^3 p_l} \sum_l a_l^3 \nabla p_l + \beta q_i p_i \nabla \phi \right), \text{ in } \Omega_s,\ i = 1, \ldots, K. \tag{3}$$

$$-\nabla \cdot \epsilon \nabla \phi = \rho^f + \lambda \sum_{i=1}^{K} q_i p_i, \text{ in } \Omega \tag{4}$$

where $k_i = \frac{a_i^3}{a_0^3}$ and a_i denotes the size of ith ion species and a_0 of the water molecule. A stable algorithm is required to solve the PNP-like equations on practical biophysical systems. In addition, due to the expensive computations, finite element computing softwares need to be parallelized. To improve accuracy of the solution, one may introduce adaptive strategy, which greatly complicates the implementation. Finally, more theoretical analysis on finite element method needs to be performed for the PNP theory, which is crucial for assuring the reliability and performance of numerical computations.

In this paper, not all problems listed above have been fully solved, but we have obtained several satisfactory results via introducing stable algorithms, efficient relaxation strategies, mesh adaptation and parallelization. Our work is mainly on the following aspects: (i) Based on the (generalized) Slotboom variables, we find stable algorithms for PNP and SMPNP equations; (ii) Relaxation strategies are introduced to accelerate iterations between the coupling equations; (iii) A parallel adaptive finite element code is implemented and numerical experiments indicate its high parallel efficiency; (iv) We use an *a posteriori* error estimator to control mesh adaptation and validate it by numerical tests; (v) The effectiveness and flexibility of higher order finite element elements are shown in our numerical studies. (vi) Numerical tests are performed not only on sphere cavity model but also on real biophysical systems.

The paper is organized as follows. The numerical algorithms are presented in Section 2, where Section 2.1 and Section 2.2 describe the boundary conditions and derive the weak forms of the PNPEs, Section 2.3 describes the primitive method and under-relaxation techniques, Section 2.4 and Section 2.5 introduce the Slotboom variables for the PNPEs and the generalized Slotboom variables for the size-modified PNPEs respectively, and Section 2.6 presents the mesh adaptation algorithm. The numerical results are given in Section 3, including comparisons of the primitive and transformed methods, effectiveness of mesh adaptation and high order elements, and parallel efficiency. Finally conclusions are given in Section 4.

2. Numerical Algorithms

2.1. Boundary Conditions

For the Poisson equation, the electrostatic potential strength of the outer boundary of the whole calculation domain almost vanishes because it is far away from macro-biomolecule(s) in our computation setup, i.e. $\phi = 0$ on $\partial\Omega$.

For the Nernst-Planck equation, both $\partial\Omega$ and Γ_m should be considered. p_{bulk} is set on $\partial\Omega$ as Dirichlet boundary condition, where p_{bulk} denotes the bulk concentration. In this paper, we consider the solution of the diffusion-reaction

system, which can be modeled by defining a "reactive" boundary patch Γ_a (see Figure 1), and setting the boundary conditions as follows: For the reactive species i, we have

$$p_i = 0, \text{ on } \Gamma_a; \quad n \cdot j_i = 0, \text{ on } \Gamma_m \backslash \Gamma_a \tag{5}$$

and for non-reactive species, the boundary condition can be written as

$$n \cdot j = 0, \text{ on } \Gamma_m \tag{6}$$

where $j = D(\nabla p + \beta \nabla (q\phi)p)$. The diffusion-controlled reaction rate coefficient is calculated by $k = \dfrac{-\int_{\Gamma_a} n \cdot j ds}{p_{\text{bulk}}}$. This boundary condition models the fact that the diffusion time scale is much larger than the reactive time scale and that in the solution there is a sufficient large number of solute molecules which are able to hydrolyze all ligands that migrate to the reaction centers of solute molecules. The non-zero flux on the reactive surface makes the particle concentrations described by PNP differ fundamentally from the Boltzmann distribution, which can be reproduced if the macroscopic flux is vanishing everywhere [45].

2.2. Finite Element Discretization

A tetrahedral mesh is used to discretize the whole domain Ω, and the molecular surface is defined by a surface mesh of triangles on both Γ_m and Γ_s.
To solve the PE, we divide ϕ into three parts, the singular component G of the electrostatic potential, a harmonic component H and the regular component ϕ_r as [10,33]

$$\phi = G + H + \phi_r. \tag{7}$$

We define the singular component G to be the restriction on Ω_m of the solution of

$$-\nabla \cdot \epsilon_m \nabla G = \rho^f, \text{ in } \mathbb{R}^3 \tag{8}$$

and harmonic component H to be the solution of a Laplace equation

$$-\Delta H = 0, \text{ in } \Omega_m \tag{9}$$

$$H = -G, \text{ on } \Gamma_m \tag{10}$$

It is seen that G can be given analytically by Green's function

$$G = \sum_k \frac{q_k}{\epsilon_m 4\pi r_k}, \tag{11}$$

where q_k is the kth atomic charge and r_k is the distance from current position to the kth atom. This G is then used to compute the boundary condition for H, the latter is to be solved numerically from Eq. (9), for which we use a finite element method in this study. It is worth noting that there is no decomposition of the potential in the solvent region, thus $\phi(x) = \phi_r(x)$ in Ω_s. Two interface conditions on Γ_m need to be satisfied according to the physical laws:

$$[\phi] = \phi_s - \phi_m = 0 \tag{12}$$

$$[\epsilon \frac{\partial \phi}{\partial n}] = \epsilon_s \frac{\partial \phi_s}{\partial n} - \epsilon_m \frac{\partial \phi_m}{\partial n} = 0 \tag{13}$$

where $[\cdot]$ denotes the jump on Γ_m of enclosed quantity from Ω_m to Ω_s. Substituting two components from Eq. (2) we get the governing equation for the regular component ϕ_r:

$$-\nabla\cdot\epsilon\nabla\phi_r = \lambda\sum_i q_i p_i, \text{ in } \Omega_m\cup\Omega_s \tag{14}$$

$$[\phi_r]=0, [\epsilon\frac{\partial\phi_r}{\partial n}] = \epsilon_m(\frac{\partial G}{\partial n}+\frac{\partial H}{\partial n}), \text{ on } \Gamma_m \tag{15}$$

Let $u = e_c\beta\phi_r$, with boundary conditions given in Section 2.1, the weak form of the PE is derived as follows:
Find $u\in H_0^1(\Omega)$ which satisfies

$$\int_\Omega(\epsilon\nabla u\nabla v)d\Omega = e_c\beta\left(\int_\Omega\lambda\sum_i(q_ip_i)vd\Omega-\epsilon_m\int_{\Gamma_m}(\frac{\partial G}{\partial n}+\frac{\partial H}{\partial n})vd\Gamma_m\right),\ \forall v\in H_0^1(\Omega) \tag{16}$$

The weak form of the NP is obtained as follows:
Find $p_i\in H^1(\Omega_s)$ which satisfies

$$\int_{\Omega_s}(\nabla p_i\nabla v + z_ip_i\nabla u\nabla v)d\Omega_s = 0,\ \forall v\in H_0^1(\Omega_s) \tag{17}$$

$$p_i|_{\partial\Omega} = p_{\text{bulk}},\ \text{i} = 1,\ 2,\ 3. \tag{18}$$

$$n\cdot j_i|_{\Gamma_m} = 0,\quad i=1,2. \tag{19}$$

$$n\cdot j_3|_{\Gamma_m\setminus\Gamma_a} = 0,\quad p_3|_{\Gamma_a} = 0 \tag{20}$$

Three kinds of diffusing species are considered in this paper, therefore we set $K = 3$. In our numerical studies, the first two kinds of species are non-reactive and the third is reactive, therefore all of them have same boundary conditions on $\Gamma_m\setminus\Gamma_a$ as described in Eq. (19) while different on Γ_a as described in Eq. (20). Of course, we also consider in this paper the case of no reactive species, then Eq. (20) is ignored and $K = 2$.
Compared to the original model with a fixed charge source distribution, the regularized PNP equations have different features [33]. Firstly, the decomposition of electrostatic potential only occurs inside biomolecules, thus the numerical solution of ϕ_r in Ω_s no longer suffers the instability. Secondly, the singular and harmonic components only need to be solved once *a priori* before the coupled solutions of the regularized PNPEs. They serve only for providing fixed interface conditions for solving ϕ_r.

2.3. Primitive Iterative Strategies for the Coupled Systems

The solution of the PNPEs is obtained by finding the fixed point of the system which couples electrostatic potential and ion concentrations. Since the equations solved within each iteration are linear, the iterative algorithm as described in Algorithm 1 can be considered as another approach to solve the nonlinear Poisson-Boltzmann equation in steady state. To our experience, to improve convergence rate, under-relaxation should be employed [13], especially when macromolecule exists. In the literature, over-relaxation has been used in the finite difference solver [31] but it is found not applicable in this context. The error tolerance tol > 0 and relaxation coefficient $0 < \alpha < 1$ are predefined constants. Since it costs several tens or hundreds iterations by using Algorithm 1 to converge to a reasonable solution, DIIS method is employed here to accelerate convergence. DIIS (direct inversion of the iterative subspace) method, which is an extrapolation technique and also a dynamic relaxation method, was developed by Péter Pulay in the field of computational quantum chemistry with the intent to accelerate and stabilize the convergence of the Hartree Fock self consistent field method [41]. Briefly, the approach uses a linear combination of approximate error vectors from previous iterations.
Given a system $\mathcal{S}$, ρ_{in} denotes the input of $\mathcal{S}$ and ρ_{out} the output. The stopping criterion is set as $\|\rho_{\text{in}}-\rho_{\text{out}}\| < \text{tol}$. Simple mixing and Anderson mixing are two general DIIS methods described as follows:

Algorithm 1 Primitive iterative method for PNP

for each $i \in [1, K]$ **do**
  Initialize ion density $p_i = 0$ and auxiliary variable $\hat{p}_i = 0$;
end for
Initialize electrostatic potential $u = 0$ and auxiliary variable $\hat{u} = -1$;
while $\|u - \hat{u}\|_2 >$ tol **do**
  Determine $\hat{u}$ as electrostatic potential of the PE by using p_i as ion densities;
  $u \longleftarrow \alpha u + (1-\alpha)\hat{u}$;
  for each $i \in [1, K]$ **do**
    Determine $\hat{p}_i$ as ion densities of the NP by using u as electrostatic potential;
    $p_i \longleftarrow \alpha p_i + (1-\alpha)\hat{p}_i$
  end for
end while

- Simple Mixing
  ρ_{in}^n denotes the n-th step input of system $\mathcal{S}$, then the next input is calculated as

$$\rho_{\text{in}}^{n+1} = (1-\alpha)\rho_{\text{in}}^n + \alpha\rho_{\text{out}}^n \tag{21}$$

  It is so called *under-relaxation* if $0 < \alpha < 1$ and *over-relaxation* if $\alpha > 1$.

- Anderson Mixing
  Define $F(\rho) = \rho_{\text{out}} - \rho_{\text{in}}$, $\rho_{\text{in}}^{\text{opt}} = (1-\beta)\rho_{\text{in}}^n + \beta\rho_{\text{in}}^{n-1}$, $\rho_{\text{out}}^{\text{opt}} = (1-\beta)\rho_{\text{out}}^n + \beta\rho_{\text{out}}^{n-1}$ where β is the solution of the least square problem:

$$\min_{\beta} \left\| \rho_{\text{in}}^{\text{opt}} - \rho_{\text{out}}^{\text{opt}} \right\|_2 \tag{22}$$

  It can be solved as:

$$\begin{aligned}
\min_{\beta} \left\| \rho_{\text{in}}^{\text{opt}} - \rho_{\text{out}}^{\text{opt}} \right\|_2 &= \min_{\beta}(\rho_{in}^{opt} - \rho_{out}^{opt}, \rho_{in}^{opt} - \rho_{out}^{opt}) \\
&= \min_{\beta}((1-\beta)\rho_{in}^n + \beta\rho_{in}^{n-1} - (1-\beta)\rho_{out}^n - \beta\rho_{out}^{n-1}, (1-\beta)\rho_{in}^n + \beta\rho_{in}^{n-1} - (1-\beta)\rho_{out}^n - \beta\rho_{out}^{n-1}) \\
&= \min_{\beta}(F^n - \beta(F^n - F^{n-1}), F^n - \beta(F^n - F^{n-1})) \\
&= \min_{\beta}\left\{(F^n, F^n) - 2\beta(F^n, F^n - F^{n-1}) + \beta^2(F^n - F^{n-1}, F^n - F^{n-1})\right\}
\end{aligned}$$

  as $(F^n - F^{n-1}, F^n - F^{n-1}) > 0$, therefore a unique solution is obtained:

$$\beta = \frac{(F^n, F^n - F^{n-1})}{(F^n - F^{n-1}, F^n - F^{n-1})} \tag{23}$$

  The next step input is written as

$$\rho_{\text{in}}^{n+1} = (1-\alpha)\rho_{\text{in}}^{\text{opt}} + \alpha\rho_{\text{out}}^{\text{opt}} \tag{24}$$

Anderson Mixing is more complicated than Simple Mixing due to its extra calculations of β as described in Eq. (23), therefore it should be applied to accelerate the iterations only if Simple Mixing does not converge or has a very low convergence rate.

2.4. A Symmetric Transformation of PNPEs

The discretization of the Nernst-Planck equation described in Algorithm 1 leads to an asymmetric weak form. A general treatment to get a symmetric weak form, which is widely used in the study of semiconductor devices, is to employ the Slotboom variables [42,27,28]. It is seen that by introducing the Slotboom variables

$$P_i = p_i e^{q_i\beta\phi_r}, \qquad \hat{D}_i = D_i e^{-q_i\beta\phi_r}, \tag{25}$$

the Nernst-Planck equation can be transformed as

$$\frac{\partial(P_i e^{-q_i\beta\phi_r})}{\partial t} = \nabla\cdot(\hat{D}_i\nabla P_i) \tag{26}$$

These transformations hence give rise to a self-adjoint, uniformly elliptic operator in the case of a fixed potential. When we consider steady-state diffusion, the left side of Eq. (26) is 0. The application of transformations in Eq. (25) to the steady-state diffusion will lead to weak forms as

$$\int_{\Omega_s}(\hat{D}_i\nabla P_i\nabla v)d\Omega_s = 0, \tag{27}$$

$$\int_{\Omega}(\epsilon(r)\nabla\phi_r\nabla v)d\Omega = \left(\int_{\Omega_s}\sum_i(z_i e^{-q_i\beta\phi_r}P_i)v\,d\Omega_s - \int_{\Gamma_m}(\frac{\partial G}{\partial n}+\frac{\partial H}{\partial n})v\,d\Gamma_m\right), \tag{28}$$

where P_i and ϕ_r are unknowns in the transformed system. After getting approximations of P_i when converged, the concentrations of PNP system are obtained by $p_i = P_i e^{-q_i\beta\phi_r}$. Compared with the original PE, these transformations lead to a nonlinear part of potential field and the Newton method is used here to solve Eq. (28). Therefore, we have two nested levels of iterations:

- Internal iterations: iterations for solving the nonlinear PE using Newton method;
- External iterations: iterations between the NP and PE.

Denote by $\{\Phi_j \mid j = 1,\ldots,N\}$ the finite element bases. Let ϕ_r^m be the finite element approximation of ϕ_r at the mth Newton iteration, which can be regarded as a vector in $\mathbb{R}^N$ composed of its degrees of freedom. We define a nonlinear function $F(\phi_r^m)$ ($\mathbb{R}^N\to\mathbb{R}^N$) whose jth component is given by:

$$F(\phi_r^m)_j = \int_{\Omega}(\epsilon\nabla\phi_r^m\nabla\Phi_j)d\Omega - \int_{\Omega_s}\sum_i(z_i e^{-q_i\beta\phi_r^m}P_i)\Phi_j d\Omega_s + \int_{\Gamma_m}(\frac{\partial G}{\partial n}+\frac{\partial H}{\partial n})\Phi_j d\Gamma_m \tag{29}$$

Then the Newton iteration of the Poisson equation reads

$$F'(\phi_r^m)(\phi_r^m - \phi_r^{m+1}) = F(\phi_r^m), \tag{30}$$

where $F'(\phi_r^m)$ is the Jacobian matrix whose j,l-th element is given by:

$$F'(\phi_r^m)_{j,l} = \int_{\Omega}(\epsilon\nabla\Phi_l\nabla\Phi_j)d\Omega + \int_{\Omega_s}\sum_i(q_i\beta P_i e^{-q_i\beta\phi_r^m})\Phi_l\Phi_j d\Omega_s$$

As described in Algorithm 1, the under-relaxation techniques can also be applied here to the iterations between the transformed NPEs and PE (Eqs. (??-28)).

2.5. A Symmetric Transformation of the Size-modified PNPEs

Our primitive algorithm fails to solve the size-modified Poisson-Nernst-Planck equations (SMPNP) [35] except in simple cases like the sphere model. By introducing new Slotboom variables [37], the SMPNP equations applied to real protein systems and the DNA fragment system have been successfully solved in this work. Eq. (3) adds size effects into models and can also be transformed to give rise to self-adjoint, uniformly elliptic operator in case of a fixed potential. Here we introduce the following transformations

$$P_i = p_i e^{q_i\beta\phi_r}(1-\sum_l a_l^3 p_l)^{-k_i}, \qquad \hat{D}_i = D_i e^{-q_i\beta\phi_r}(1-\sum_l a_l^3 p_l)^{k_i} \tag{31}$$

as a set of generalized Slotboom variables for our SMPNP system, the weak form of the steady-state size-modified PNPEs reads

$$\int_{\Omega_s}\left(\hat{D}_i\nabla P_i\nabla v\right)d\Omega_s = 0 \tag{32}$$

$$\int_{\Omega}(\epsilon(r)\nabla\phi_r\nabla v)d\Omega = \left(\int_{\Omega_s}\sum_i(q_i e^{-q_i\beta\phi_r}(1-\sum_l a_l^3 p_l)^{k_i}P_i)v\,d\Omega_s - \int_{\Gamma_m}(\frac{\partial G}{\partial n}+\frac{\partial H}{\partial n})v\,d\Gamma_m\right) \tag{33}$$

where only P_i and ϕ_r are solved as unknowns. For each external iteration between the NP and PE, we approximates $p_i^n = P_i^n e^{-q_i\beta\phi_r}(1-\sum_l a_l^3 p_l^{n-1})^{k_i}$, where p_i^n denotes the update in the nth external iteration. When converged, it satisfies $p_i = P_i e^{-q_i\beta\phi_r}(1-\sum_l a_l^3 p_l)^{k_i}$. As with the original PNPE, this transformation leads to a nonlinear Poisson equation for the potential field and the Newton method is used to solve Eq. (33). Here the nonlinear function $F(\phi_r^m)$ is defined by:

$$F(\phi_r^m)_j = \int_{\Omega}(\epsilon\nabla\phi_r^m\nabla\Phi_j)d\Omega - \int_{\Omega_s}\sum_i(z_i e^{-q_i\beta\phi_r^m}(1-\sum_l a_l^3 p_l)^{k_i}P_i)\Phi_j d\Omega_s + \int_{\Gamma_m}(\frac{\partial G}{\partial n}+\frac{\partial H}{\partial n})\Phi_j d\Gamma_m, \tag{34}$$

and the Newton iteration of the Poisson equation reads

$$F'(\phi_r^m)(\phi_r^m-\phi_r^{m+1}) = F(\phi_r^m) \tag{35}$$

where

$$F'(\phi_r^m)_{j,s} = \int_{\Omega}(\epsilon\nabla\Phi_s\nabla\Phi_j)d\Omega + \int_{\Omega_s}\sum_i(q_i\beta P_i e^{-q_i\beta\phi_r^m}(1-\sum_l a_l^3 p_l)^{k_i})\Phi_s\Phi_j d\Omega_s$$

It is worth noting that in the traditional PNPEs, $\hat{D}$ is only dependent on the potential u, but not on the concentration p. Thus, for a given u, the stiffness matrix of the PE is symmetric. While in size-modified PNPEs, $\hat{D}$ is dependent both on the potential u and on the unknown concentration p. In numerical computation of $\hat{D}$ in each iteration , we shall use p_i^{n-1} as the concentration distribution to maintain the size-modified NPE symmetric.

2.6. Mesh Adaptation

Adaptive mesh refinement is an effective method for improving the accuracy of the numerical solution in finite element computations. Here we employ the so called *h-refinement* [3] using an *a posteriori* error estimate to PNPEs, which consists of the following steps:

Solve compute the finite element solution for the harmonic component H, the potential and concentration distribution on the current mesh as described in Section 2.3

Estimate compute an elementwise *a posteriori* error indicator on each element using the current numerical solution

Mark select a subset of elements on which the error indicators are large

Refine refine (subdivide) the selected elements, plus possibly more elements to maintain the conformity of the mesh

The above steps are repeated until some criteria are met, which would eventually produce a quasi-optimal mesh for solving the given problem. In this paper bisection is used to refine (subdivide) an element. This method is widely used in recent researches [22,25,9].
A crucial ingredient for the effectiveness of mesh adaptation is the *a posteriori* error estimate used to calculate the error indicators. In this paper we use the following formula to compute the error indicator η_s on the element s

$$\eta_s = \left(h_s^2 \left\| \sum_i q_i p_i + \rho^f + \nabla \cdot (\epsilon \nabla \phi_h) \right\|_{L^2(s)}^2 + \frac{1}{2} \sum_{f \in F(s)} h_f \left\| [(\epsilon \nabla \phi_h) \cdot n_f] \right\|_{L^2(f)}^2 \right)^{\frac{1}{2}}, \tag{36}$$

in which $F(s)$ denotes the set of (non-boundary) faces of s, h_s the diameter of s, h_f the diameter of the face f, n_f the normal of the face f, and $[\cdot]$ the jump of the enclosed quantity across the face f. The reasons why we define the error indicator as in Eq. (36) rather than considering the NP equations mainly rely on: (i) The magnitude of concentrations varies a lot and differs much from the potential, so does its *a posteriori* error estimation. Therefore an estimator combining both potential and concentrations to control mesh refinement is hard to define. (ii) If $\|u_{h1} - u_{h2}\| < tol$ and tol is small enough, then the concentrations must be very closed since the system is coupling of the two fields.
The above error indicator is similar to the well-known *a posteriori* error indicator for the Poisson-Boltzmann equation introduced by [22] if we consider steady-state diffusion process for the case of two ion sizes. It reflects the residue of the PE and the jump discontinuities in the dielectric are detected by the second term in the sum containing the jump function, leading to mesh refinement at the dielectric boundary. The following theorem justifies the validity of this error indicator in the NPBE system [22].

Theorem 1.
Let ϕ and ϕ_h be the exact and numerical solutions of electrostatic potential of the NPBEs respectively, here $\phi_h \in V_h$ and V_h denotes the standard H^1-conforming linear finite element space, then the following a posteriori *error estimate holds:*

$$\left\| \phi - \phi_h \right\|_{H^1_\Omega} \leq C_0 \left(\sum_{s \in \mathcal{M}} \eta_s^2 \right)^{\frac{1}{2}}, \tag{37}$$

where $\mathcal{M}$ denotes the tetrahedral mesh, C_0 is a constant depending on the discretization.

The error indicator defined in Eq. (36) is an extension for the case of three ion sizes in the steady-state diffusing process. Its effectiveness for adaptive refinements is discussed in Section 3.4.
The mesh adaptation algorithm is described in Algorithm 2, in which the error tolerance tol > 0 is a predefined constant.

Algorithm 2 The mesh adaptation algorithm

Initialize an initial mesh $\mathcal{M}_0$;
Solve the discrete problem of the PNPEs on $\mathcal{M}_0$;
Compute the local error indicator η_s on each $s \in \mathcal{M}_0$;
Set $k = 0$;
while $err_k = (\sum_{s \in \mathcal{M}_k} \eta_s^2)^{\frac{1}{2}} >$ tol **do**
  Refine all $s \in \mathcal{M}_k$ satisfying $\eta_s > \frac{1}{2} max_{s \in \mathcal{M}_k} \eta_s$ to construct a conforming mesh $\mathcal{M}_{k+1}$, plus a few more to maintain mesh conformity;
  Solve the discrete problem of the PNPEs on $\mathcal{M}_{k+1}$;
  Compute the local error indicator η_s on each $s \in \mathcal{M}_{k+1}$;
  Set $k = k + 1$;
end while

3. Numerical Results

In this section, we apply the adaptive finite element algorithms presented in the last section to the sphere cavity model and protein systems to study the electrostatic potential, ion concentrations and reactive rate constants under various combinations of inputs. Various aspects of the algorithms including the convergence rate of linear and nonlinear solvers,

the effectiveness of mesh adaptation and the parallel efficiency and scalability of the parallel code are demonstrated using these systems.

The implementation of the algorithms is based on the parallel adaptive finite element package PHG [53]. The parallel code is written in C and uses MPI for message passing. The computations were carried out on the cluster LSSC-III of the State Key Laboratory of Scientific and Engineering Computing of China, which consists of compute nodes with dual Intel Xeon X5550 quad-core CPUs, interconnected via DDR InfiniBand network.

3.1. Reaction Rate Coefficients: ACh-AChE System

One of the protein systems computed here is the acetylcholine (ACh)–acetylcholinesterase (AChE) system. The surrounding solvent domain is a sphere with a radius of 400 Å. Detailed description of the system can be found in [36]. We compute the reaction rate coefficients of neurotransmitter ACh at the reaction center of the enzyme AChE. The molecular surface of which is schematically illustrated in Figure 2. This system carries a total fixed charge of $-7.61e_c$. The mesh over the whole domain has a total of 176 673 vertices and 1 099 255 tetrahedra. The coefficient ϵ is piecewise constant in the computational domain which equals to $\epsilon_m = 2$ in Ω_m and $\epsilon_s = 78$ in Ω_s. The diffusion coefficient $D = 78000$ Å^2/µs. Steady state simulations are performed in this work to calculate the reaction rate coefficients under different conditions.

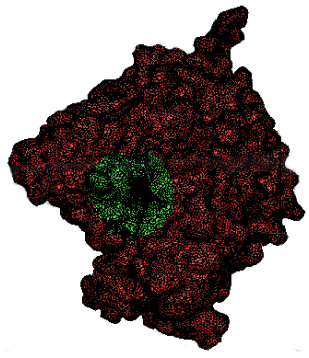

Fig 2. The discretized molecular surface of AChE with the region around the reaction center colored green, which is generated by TetView [49].

We assume that there are only monovalent ions in the salt, C_1 and C_2 are the total bulk concentrations of cation and anion respectively, and C_{sub} is the bulk concentration of substrate. These bulk values are used as Dirichlet conditions of the diffusion domain in solving the PNPEs. Therefore, to make a closer connection with physiology, it is reasonable to consider a neutrality condition of the bulk values in our work as $q_1C_1 + q_2C_2 + q_3C_{\text{sub}} = 0$, where $q_1 = +1e_c$ and $q_2 = -1e_c$ and they denote the charges of non-reactive species respectively. Reaction rate k depends on both ionic strength and substrate concentration. For the ACh-AChE system, $q_3 = +1e_c$.

The reaction rate constant is shown as a function of ionic strength for different prescribed substrate concentrations in Figure 3(a) (linear finite element is used).

At very low substrate concentration, i.e. 1 mM or less, the results show asymptotic agreement with the Debye-Hückel limiting law [16]. However, at moderate concentrations of the substrate, the curves are shifted. The general trend is that the the reaction rate increases as the bulk concentration of substrate increases for a fixed overall ionic strength. At very high ionic strength, due to strong Debye screening effects, the electrostatic interactions become weak. Therefore, the reaction rate reduces to a low level at different substrate concentrations, and are close to the pure diffusion-reaction rate constant.

We come to study the size effects on the reaction rate for the ACh-AChE system by using the SMPNP model that has not been successfully applied to real protein systems previously. In our numerical studies, it is found that the transformation method which leads to a self-adjoint operator is stable and robust in dealing with not only the simple sphere model, but also the protein systems. Figure 3(b) illustrates the reactive rate constants for various combinations of ionic strength and substrate concentration with $a_0 = 11.5$ Å, $a_1 = 6$ Å, $a_2 = 6$ Å and $a_3 = 8$ Å. Compared to the case illustrated in Figure 3(a) without size-effect, it is found that the predicted reaction rate coefficients of the attractive

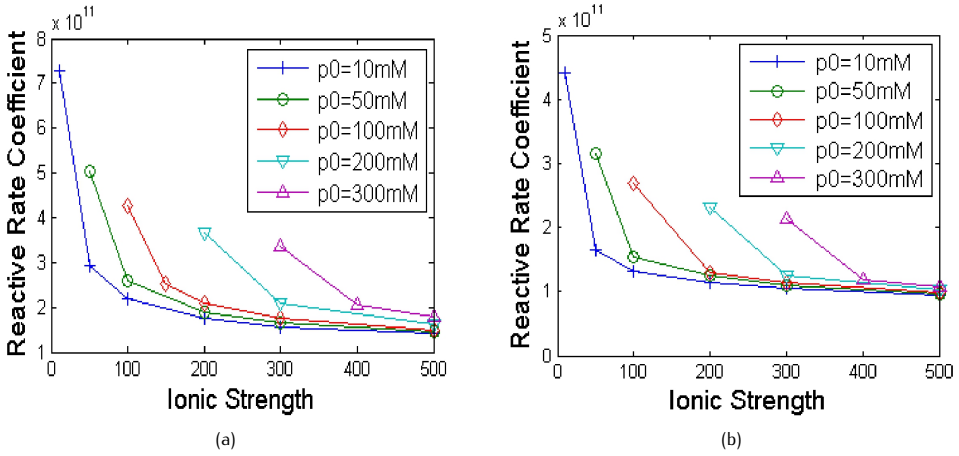

Fig 3. Reaction rate coefficient ($M^{-1}\,min^{-1}$) affected by both ionic strength and substrate concentration for the ACh-AChE system without size-effect (left) and with size-effect (right). p_0 is bulk substrate concentration (mM) and ionic strength mM) includes spectator ions plus substrate, i.e. $\frac{1}{2}(\sum_{i=1}^{2}|q_iC_i| + |q_3C_{sub}|)$.

substrate are smaller than the results from PNP model. With size effects, it can be seen from Eq. (3) that the flux is influenced by the additional coupled terms with concentration gradients of all the diffusing species. Within those, the counter-ion term is dominant due to its much higher concentration and gradient at reactive surface. And note that the counter-ion and substrate concentration gradients have opposite signs, which negates the substrate flux hence lowers the reaction rate coefficient.

3.2. Electrostatic Potential and Ion Concentrations: DNA Fragment

A DNA fragment is studied, a system which has high permanent charges and leads to numerical difficulties in convergence. There are only two species considered in the DNA fragment system and both of them are non-reactive and in an equilibrium state. Therefore the ion concentrations follow Boltzmann distributions and the PNP equations are equivalent to the Nonlinear Poisson Boltzmann equation. Figure 4 illustrates an example of the unstructured tetrahedral volume mesh and triangulated surface mesh of a fragment of A-form DNA that is taken from [36]. The figures are produced by Paraview [1] and Tetgen[48].

The system carries total fixed charge of $-22e_c$. It has a strong negative potential field, which attracts cations. The mesh over the whole domain has a total of 99 093 vertices and 620 117 tetrahedra, with 24 503 vertices and 49 002 triangles on the molecular surface. The system is bounded on the outside by a spherical boundary with a radius of 200 Å.

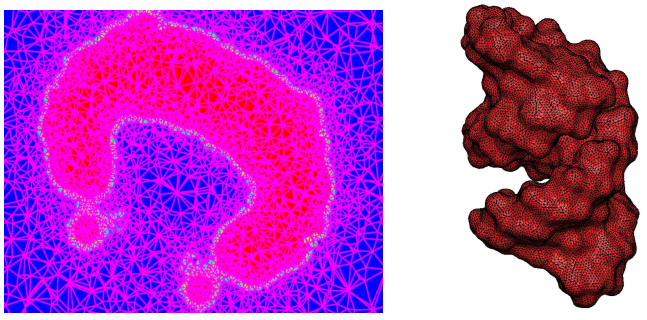

Fig 4. An example mesh for a fragment of A-form DNA. (a) A close-up view of the fine mesh around the molecule. (b) The triangular boundary mesh conforming to the molecular surface.

Both the bulk densities of Na^+ and Cl^- are set to 50 mM. Figure 5 shows the electrostatic potential and corresponding ion density distributions, by which we can notice that the electrostatic potential in 50 mM solution ranges from -3.63 to 0.92 k cal/mol $\cdot e_c$ and the cation density ranges from 0 to 23.1 M. The anion density ranges from 0 to 0.239 M, which is much smaller than cation density. High cation concentration appears in the vicinity of the molecular surface. In our previous work in [36], we studied the electrostatic potential and ion concentrations in the LPBE model.

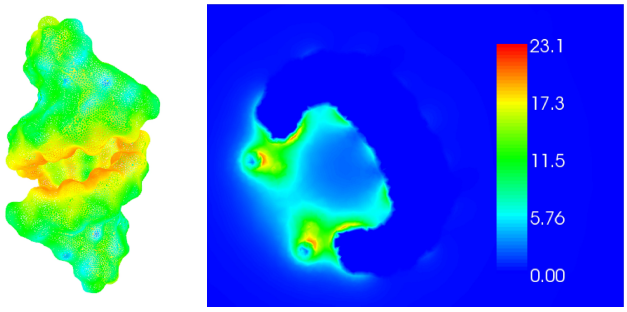

Fig 5. Electrostatic potential and cation density(M) around a fragment of A-form DNA. (a) Surface electrostatic potential from the PNPEs solution in a 50 mM salt. The color scale is from -4(red) to 1(blue) $kcal/mol \cdot e_c$. (b) Cross section of the density distribution in 50 mM NaCl solution. Notice that the cation density is defined only in solvent region.

We also studied the ion size effects on potential and densities. It can be shown that when all sizes a_i are equal, for the case of two ion sizes, it gives a very close but different form of the size-modified Poisson-Boltzmann equation [35]. According to [11], we set $a_0 = 3$ Å for the water molecule, $a_1 = 3$ Å for the positive charge species, $a_2 = 3$ Å for the negative charge species, then we have the electrostatic potential of the DNA fragment in 50 mM NaCl solution ranges from -3.78 to 0.94 $k$cal/mol $\cdot e_c$, the cation density ranges from 0 to 18.69 M. The anion density ranges from 0 to 0.236 M, which is smaller than it is in the PNPEs. When comparing the numerical results with that in the PNP case described in [36], the electrostatic potential with size-effect is found lower and the maximum counter-ion concentration drops from 23.1 M to 18.69 M while maximum co-ion concentration is not sensitive to the size effects. Obviously, the counter-ion density near the molecular surface is higher and is three or more orders larger than the co-ion density, therefore its density is sensitive to the size effects. Consistent with the observations in [37], the counter-ion density decreases and thus it contributes to a reduced screening to the electric field, hence to a higher potential.

3.3. Numerical Analysis: Convergence and Stability

The introduction of the self-adjoint electro-diffusion operator in Section 2.4 brings up a question on whether the condition number cond(A) of the PNP system increases or not after the transformations. Previous work in [33] indicates that the condition number of the stiffness matrix will have catastrophic growth as the permanent charge increases. Examples in [33] also explicitly indicate that the condition number can still be extremely large if there are positive and negative permanent charges presented inside biomolecules even if the charges are not large. Actually, it is known that the condition number with preconditioner cond(PA) is more meaningful than cond(A), where P denotes preconditioner and A the stiffness matrix. For a matrix A, cond(A) is defined as the rate of maximum and minimum eigenvalue of $A'A$. Minimum eigenvalue of $A'A$ is equivalent to maximum eigenvalue of $(A'A)^{-1}$. To compute maximum eigenvalue, we use Power Method which is widely used. Its extension to the inverse power method is practical for finding any eigenvalue provided that a good initial approximation is known. Some schemes for finding eigenvalues use other methods that converge fast, but have limited precision. We only use Power Method to analyze the condition numbers. In our numerical studies, it is more efficient to solve the NP equations in ACh-AChE system with Additive Schwarz preconditioner [50] than with ILU preconditioner [46]. In order to verify cond(PA) does not necessarily increase after transformations, numerical results on cond(PA) are calculated in the sphere cavity model, which is simpler than the ACh-AChE system, and the results show that the maximum cond(PA) during iterations on solving the NP equations for three species are 5.34×10^5 , 1.84×10^4 and 3.03×10^3 after transformations while 1.22×10^4, 3.18×10^6 and 1.26×10^2 respectively for the primitive method. For the Poisson equation, the transformed formulation is nonlinear that requires Newton iterations, thus it costs more internal iterations than the primitive formulation. Although the transformed PE causes more internal iterations of PE,

the external iterations between NP and PE can be fewer. In our studies, the primitive method described in Algorithm 1 converges at a much slower rate than the transformation method for solving the PNPEs for both the sphere cavity model and ACh-AChE system, which is demonstrated in Table 1. The comparisons made here are under the same condition of using same relaxation parameters $\alpha = 0.1$ in the external iterations.

Table 1. CPU time costs (with 32 processors) and external iterations between the NP and the PE under different combinations of ionic strength (mM) and substrate concentration (mM) for the sphere cavity model and the ACh-AChE system.

Ionic strength and substrate concentration (mM)	Sphere Cavity model		ACh-AChE system	
	primitive	transformed	primitive	transformed
50 mM, 10 mM	149 (23.06 s)	3 (2.54 s)	148 (1072.88 s)	10 (168.82 s)
50 mM, 50 mM	152 (23.91 s)	3 (2.66 s)	154 (1114.3 s)	14 (230.91 s)
100 mM, 50 mM	145 (21.57 s)	3 (2.63 s)	141 (1018.24 s)	12 (200.92 s)
300 mM, 10 mM	148 (21.92 s)	3 (2.39 s)	153 (1108.06 s)	8 (128.94 s)
300 mM, 50 mM	148 (22.14 s)	3 (2.68 s)	151 (1092.59 s)	9 (146.44 s)
300 mM, 100 mM	148 (22.22 s)	3 (2.74 s)	149 (1080.12 s)	10 (167.88 s)

In the sphere cavity model, the number of internal iterations of the transformed PE ranges from 2 to 5, and the total number of iterations is less than 20 in each PNP solution. The changes in condition number for the transformed PE are not significant. Compared to the sphere model, the ACh-AChE model has larger total permanent charges $Q = -7.61e_c$ and the number of iterations between the transformed NP and PE increases but is still much smaller than the primitive method. It is worth noting that the number of internal iterations of the transformed PE ranges from 2 to 13, and it costs about several tens iterations to solve each system in total. In other words, for above two systems, self-adjointness of the electro-diffusion operator significantly improves the convergence rate of external iterations compared to the primitive method. Table 1 shows the transformed method decreases CPU time by 80% compared to the primitive method in the meanwhile.

It is worth noting that the transformation method causes a rapid growth of the internal iterations in our numerical studies of different systems, although it only takes several external iterations between the NP and the PE. It is also found that the reactive boundary condition is always associated with a smaller condition number than the non-reactive boundary condition. From our observations, it is seen that the transformation method with Algorithm 1 is stable for solving practical systems but sometimes it costs many internal iterations when solving the nonlinear transformed PE.

The two under-relaxation methods, Simple Mixing and Anderson Mixing, described in Section 2.3, are static and dynamic choices of relaxation coefficient respectively. In addition to Simple Mixing, we also have numerical experiments to study how Anderson Mixing accelerates the iterations between the NP and the PE in primitive method. It is worth noting that we only use Anderson Mixing on potential field but still use Simple Mixing on concentration field rather than apply Anderson Mixing on both fields. Because using Anderson Mixing on both fields will not make significant acceleration and may cause divergence under some combinations of parameters meanwhile. Table 2 illustrates the results with and without Anderson Mixing for the sphere cavity model at low concentration 1:1 salt solution.

Table 2. Comparisons on the number of iterations with and without Anderson Mixing via using primitive method for the sphere cavity model.

Ionic strength and substrate concentration (mM)	Iterations by Simple Mixing	Iterations by Anderson Mixing
1 mM, 1 mM	154	57
10 mM, 10 mM	153	57
10 mM, 5 mM	144	81
10 mM, 1 mM	154	53
50 mM, 50 mM	152	104
50 mM, 10 mM	149	93
100 mM, 100 mM	153	113
100 mM, 50 mM	145	127
100 mM, 10 mM	150	102

It is seen that the number of iterations using Anderson Mixing as under-relaxation strategy is smaller than using Simple Mixing and the former does accelerate convergence of the iterations between the NP and the PE at low concentrations. Our results indicate that the accelerations are not significant at high concentrations for the sphere cavity model. However,

the primitive method with Anderson Mixing still costs more external iterations than the transformed method with Simple Mixing, which can be observed from Table 1 and Table 2.

3.4. Mesh Adaptation

To demonstrate the effectiveness of mesh adaptation, we apply Algorithm 2 to the sphere cavity model. Figure 6 shows the decay rates of the *a posteriori* error estimate (y axis) with respect to the number of degrees of freedom (DOFs, x axis) for the PNP system in the mesh adaptation procedure. The optimal error decay rate is indicated by a line of slope $-1/3$ for the linear element used in the computations. We observe that on the adaptive meshes the error decay rates are quasi-optimal. For uniform refinements, we compute the error decay and found it can not reach the quasi-optimal convergence. Figure 7 compares the error estimates between uniform refinements and adaptive refinements when $Is = 50$ mM and $p_{bulk} = 50$ mM for the steady-state diffusing case. From Figure 7, we can make conclusions as follows: (i) For a given tolerance of the error estimates, adaptive refinements will reach the tolerance with less degrees of freedom (DOFs). (ii) If the stop criterion of refinements is a given upper bound memory of mesh grid size, then adaptive refinements will get better accuracy. (iii) After 2-3 uniform refinements, the decay rate of error estimates becomes flatter than before. Therefore, mesh adaptation is necessary if we want to get better FEM approximations via mesh refinements.

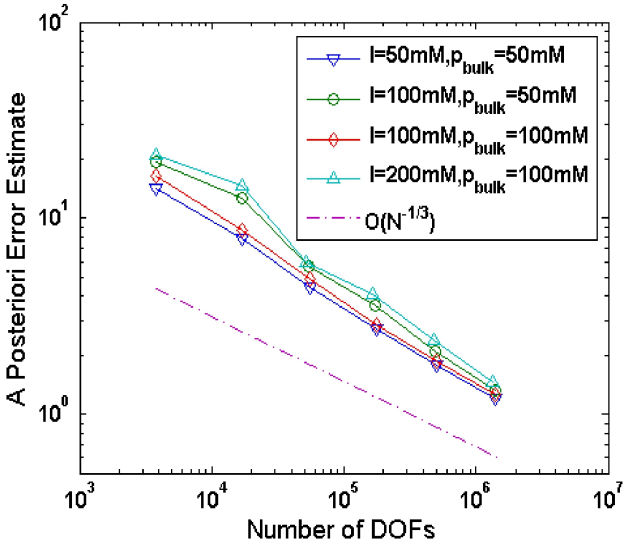

Fig 6. The quasi-optimal convergence of the mesh adaptation algorithm for various combinations of ionic strength (mM) and substrate concentration (mM) in the sphere cavity model, which is indicated by a line of slope $-1/3$ in the case of linear element.

3.5. Parallel Scalability and Efficiency

To assess the parallel scalability and efficiency of our parallel code, we introduce a much larger system with a mesh containing a total of 2 800 768 vertices and 17 522 738 tetrahedra, on which we solve the PNPEs using the transformed method and quadratic element. The total number of unknowns is 23 134 140. For the solution of the linear systems, we use PCG as solver because of its symmetry. Table 3 gives the wall-clock time and parallel efficiency for different number of MPI processes. Due to large memory requirements, our tests start with 64 processes, whose parallel efficiency is regarded as 100%, and the parallel efficiency for p processes is defined as

$$E_p = \frac{64 T_{64}}{p T_p}.$$

where T_p denotes the wall-clock time needed for solving the PNPEs using p processes.The parallel efficiencies obtained are satisfactory. One can notice a rapid drop in the parallel efficiency when going from 512 processes to 1 024 processes,

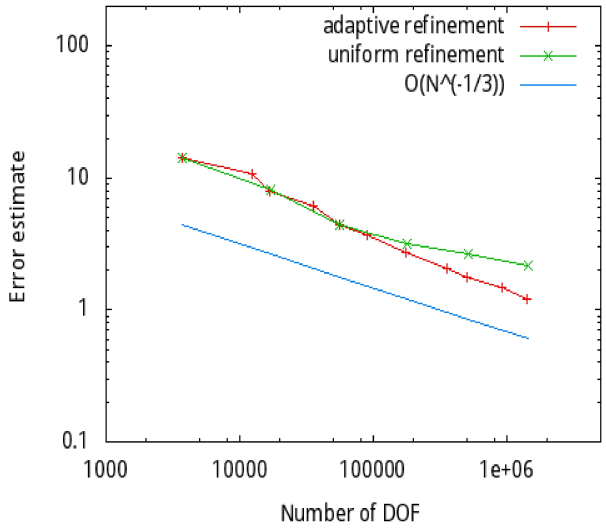

Fig 7. Comparisons of convergence between using uniform refinements and adaptive refinements. Both the numerical solutions are obtained from PNP system by setting $Is = 50$ mM and $p_{bulk} = 50$ mM.

which we believe may be related to the interconnection topology of the underlying InfiniBand network. We also expect the code to work with larger parallel computers by using faster interconnection network, solving larger problems, or exploiting the OpenMP/MPI two level parallelism provided by PHG.

Table 3. Parallel efficiency in solving the PNPEs using transformed method with solver PCG.

Num of Procs	Time (s)	Efficiency
64	1899.2	100%
128	840.6	112.9%
256	384.8	123.4%
512	221.2	107.3%
1024	176.6	67.2%

3.6. High Order Finite Elements

An interesting feature of PHG is the ability to use different finite element types without changing the code. In this section we demonstrate the effectiveness of high order elements by solving the PNPEs and SMPNPEs for the sphere cavity model using our code with linear, quadratic and cubic elements respectively.

Figure 8 illustrates the decay of error estimate of electrostatic potential under linear, quadratic and cubic elements, with respect to the number of DOF, during the uniform mesh refinement procedure. For all three elements we observe quasi-optimal error decay rates indicated by the asymptotic slopes of the curves in the figure ($-1/3$ for linear element, $-2/3$ for quadratic element and $-3/3$ for cubic element). Both quadratic and cubic elements are more efficient than the linear element in that they achieve a given error tolerance with much fewer DOF.

4. Conclusions

We have developed a parallel adaptive finite element code for solving the electro-diffusion equations with permanent charges in real biomolecular systems. We adopted a recently developed and widely used technique [10,37] to regularize the Poisson equation featured with singular charges distributed in the molecular domain in the PNP systems. By introducing Slotboom variables to the PNP and the size-modified PNP equations, the resulting self-adjoint operator is more stable and robust in terms of convergence between the Poisson equation and the Nernst-Planck equations,

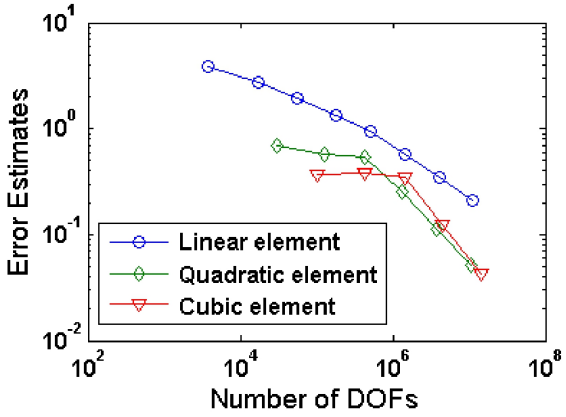

Fig 8. The error decay rates of the electrostatic potential for the sphere cavity model in a 50 mM salt with linear, quadratic and cubic elements.

which is verified by our numerical tests with practical models. The corresponding transformed Poisson equation is nonlinear which requires the Newton method and requires the iterations between the nonlinear Poisson equation and the symmetric Nernst-Planck equation to employ under-relaxation techniques. Due to the limited availability of the analytical solutions to 3D PNP, we constructed various test problems to study the electro-diffusion process and to examine the stability of the transformation method.

It's worth noting that with the primitive method, the iterations between the Poisson equation and the Nernst-Planck equations fail to converge when solving the size-modified PNP equations for protein systems. In contrast, in our numerical studies, the transformation method succeeds in converging for practical biophysical systems. By comparing the primitive method and the transformation method for the PNP equations from observations of the number of iterations between the Poisson equation and the Nernst-Planck equation and CPU time costs, it is found that the number of iterations using transformation method is significantly reduced from 150 to 3 and CPU time costs decrease by more than 80% for the sphere cavity model. Moreover, the condition numbers of the preconditioned systems for the transformation method are not significantly larger than those for the primitive method. We believe that the transformation method is more stable and robust than the primitive method for practical biophysical applications.

Our code is based on the parallel adaptive finite element package PHG. It is fully parallel with mesh adaptation and high order capability, and the advantage of mesh adaptation and high order elements has been confirmed by numerical tests. We believe our code can be applied to computations of complex, large biomolecular systems on parallel computers with thousands of CPU cores.

In this paper, we focused on the steady-state diffusion process. The parallel solution of time-dependent Poisson-Nernst-Planck equations with and without size-effect are being explored, and applications of the proposed parallel FEM algorithms to ion channels are under way.

Acknowledgements

This work was partially supported by the National Basic Research Project under the grant 2011CB309703, China NSF under the grants 10971218, 11171334 and 11021101, the National Center for Mathematics Interdisciplinary Sciences, and the Chinese Academy of Sciences. In addition, we would like to thank Bin Tu and Jingrun Chen for their helpful suggestions that improved our work.

References

[1] J. Ahrens, B. Geveci, and C. Law. Paraview: An end user tool for large data visualization. the Visualization Handbook. Edited by CD Hansen and CR Johnson. Elsevier, 2005.

[2] R. E. Bank, D. J. Rose, and W. Fichtner. Numerical methods for semiconductor device simulation. SIAM J. Sci. Statist. Comput., 4:416–435, 1983.

[3] M. J. Berger and P. Colella. Local adaptive mesh refinement for shock hydrodynamics. J. Comput. Phys., 82(1):64–84, 1989.
[4] A. H. Boschitsch and M. O. Fenley. Hybrid boundary element and finite difference method for solving the nonlinear Poisson-Boltzmann equation. J. Comput. Chem., 25(7):935–955, 2004.
[5] A. E. Cardenas, R. D. Coalson, and M. G. Kurnikova. 3D Poisson-Nernst-Planck theory studies: Influence of membrane electrostatics on gramicidin A channel conductance. Biophys. J., 79(1):80–93, 2000.
[6] D. Chen and R. Eisenberg. Charges, currents, and potentials in ionic channels of one conformation. Biophys. J., 64(5):1405–1421, 1993.
[7] Duan P. Chen. Competitive permeation of calcium ions through the calcium release channel (ryanodine receptor) of cardiac muscle: An application of the coupled Poisson-Nernst-Planck system of equations. J. Phys. Chem. B, 107(34):9139–9145, 2003.
[8] M. X. Chen and B. Z. Lu. TMSmesh: A robust method for molecular surface mesh generation using a trace technique. J. Chem. Theory Comput., 7(1):203–212, 2011.
[9] Zhiming Chen, Yuanming Xiao, and Linbo Zhang. The adaptive immersed interface finite element method for elliptic and Maxwell interface problems. J. Comput. Phys., 228(14):5000–5019, 2009.
[10] I-Liang Chern, Jian-Guo Liu, and Wei-Cheng Wang. Accurate evaluation of electrostatics for macromolecules in solution. Methods Appl. Anal., 10(2):309–328, 2003.
[11] Vincent B. Chu, Yu Bai, Jan Lipfert, Daniel Herschlag, and Sebastian Doniach. Evaluation of ion binding to DNA duplexes using a size-modified Poisson-Boltzmann theory. Biophys. J., 93(9):3202–3209, 2007.
[12] H. Cohen and J. W. Cooley. The numerical solution of the time-dependent Nernst-Planck equations. Biophys. J., 5(2):145–162, 1965.
[13] Ben Corry, Serdar Kuyucak, and Shin-Ho Chung. Dielectric self-energy in Poisson-Boltzmann and Poisson-Nernst-Planck models of ion channels. Biophys. J., 84(6):3594–3606, 2003.
[14] H. Daiguji, Y. Oka, and K. Shirono. Nanofluidic diode and bipolar transistor. Nano Lett., 5(11):2274–2280, 2005.
[15] H. Daiguji, P. Yang, and A. Majumdar. Ion transport in nanofluidic channels. Nano Lett., 4(1):137–142, 2004.
[16] P. Debye and E. Hückel. De la theorie des electrolytes. I. abaissement du point de congelation et phenomenes associes. Physikalische Zeitschrift, 24(9):185–206, 1923.
[17] B. Eisenberg, Y. Hyon, and C. Liu. Energy variational analysis of ions in water and channels: Field theory for primitive models of complex ionic fluids. J. Chem. Phys., 133:104104, 2010.
[18] R. S. Eisenberg. Computing the field in proteins and channels. J. Membr. Biol., 150(1):1–25, 1996.
[19] Q. Fang and D. A. Boas. Tetrahedral mesh generation from volumetric binary and grayscale images. In Biomedical Imaging: From Nano to Macro, 2009. ISBI'09. IEEE International Symposium on, pages 1142–1145, 2009.
[20] W. Fichtner, D.J. Rose, and R.E. Bank. Semiconductor device simulation. IEEE T. Electron Dev., 30(9):1018–1030, 1983.
[21] U. Hollerbach, D. P. Chen, D. D. Busath, and B. Eisenberg. Predicting function from structure using the Poisson-Nernst-Planck equations: sodium current in the gramicidin A channel. Langmuir, 16(13):5509–5514, 2000.
[22] M. Holst, N. Baker, and F. Wang. Adaptive multilevel finite element solution of the Poisson-Boltzmann equation i: Algorithms and examples. J. Comput. Phys., 21:1319–1342, 2000.
[23] M. J. Holst. The Poisson Boltzmann equation: Analysis and multilevel numerical solution. Ph.D thesis, University of Illinois at Urbana-Champaign, 1994.
[24] M. J. Holst. Finite element toolkit. http://www.fetk.org/, 2010.
[25] Michael Holst, Jeffrey S. Ovall, and Ryan Szypowski. An efficient, reliable and robust error estimator for elliptic problems in. Appl. Numer. Math., 61(5):675–695, 2011.
[26] W. Im and B. Roux. Ion permeation and selectivity of OmpF porin: a theoretical study based on molecular dynamics, Brownian dynamics, and continuum electrodiffusion theory. J. Mol. Biol., 322(4):851–869, 2002.
[27] A. Jungel and C. Pohl. Numerical simulation of semiconductor devices: energy-transport and quantum hydrodynamic modeling. In Computational Electronics, 1998. IWCE-6. Extended Abstracts of 1998 Sixth International Workshop on, pages 230–233, 1998.
[28] C. E. Korman and I. D. Mayergoyz. A globally convergent algorithm for the solution of the steady-state semiconductor device equations. J. App. Phys., 68(3):1324–1334, 1990.
[29] K. KrabbenhÃüft and J. KrabbenhÃüft. Application of the Poisson-Nernst-Planck equations to the migration test. Cement Concrete Res., 38(1):77–88, 2008.

[30] Witold Kucza, Marek Danielewski, and Andrzej Lewenstam. Eis simulations for ion-selective site-based membranes by a numerical solution of the coupled Nernst-Planck-Poisson equations. Electrochem. Commun., 8(3):416–420, 2006.
[31] Maria G. Kurnikova, Rob D. Coalson, Peter Graf, and Abraham Nitzan. A lattice relaxation algorithm for three-dimensional Poisson-Nernst-Planck theory with application to ion transport through the gramicidin A channel. Biophys. J., 76(2):642–656, 1999.
[32] B. Z. Lu, Y. C. Zhou, M. J. Holst, and J. A. McCammon. Recent progress in numerical methods for the Poisson-Boltzmann equation in biophysical applications. Commun. Comput. Phys., 3(5):973–1009, 2008.
[33] Benzhuo Lu, Michael J. Holst, J. Andrew McCammon, and Y.C. Zhou. Poisson-Nernst-Planck equations for simulating biomolecular diffusion-reaction processes I: Finite element solutions. J. Comput. Phys., 229(19):6979–6994, 2010.
[34] Benzhuo Lu and J. Andrew McCammon. Molecular surface-free continuum model for electrodiffusion processes. Chem. Phys. Lett., 451(4-6):282–286, 2008.
[35] Benzhuo Lu and Y.C. Zhou. Poisson-Nernst-Planck equations for simulating biomolecular diffusion-reaction processes II: Size effects on ionic distributions and diffusion-reaction rates. Biophys. J., 100(10):2475–2485, 2011.
[36] Benzhuo Lu, Y.C. Zhou, Gary A. Huber, Stephen D. Bond, Michael J. Holst, and J. Andrew McCammon. Electrodiffusion: A continuum modeling framework for biomolecular systems with realistic spatiotemporal resolution. J. Chem. Phys., 127(13), 2007.
[37] Benzhuo Lu and Yongcheng Zhou. Poisson-Nernst-Planck equations for simulating biomolecular diffusion-reaction processes II: Size effects on ionic distributions and diffusion-reaction rates. Biophys. J., 100(10):2475–2485, 2011.
[38] P.A. Markowich. The stationary semiconductor device equations, volume 1. Springer Verlag, 1986.
[39] A. Nicholls and B. Honig. A rapid finite difference algorithm, utilizing successive over-relaxation to solve the Poisson-Boltzmann equation. J. Comput. Chem., 12(4):435–445, 1991.
[40] Juan Manuel Paz-GarcÃŋa, BjÃűrn Johannesson, Lisbeth M. Ottosen, Alexandra B. Ribeiro, and JosÃĺ Miguel RodrÃŋguez-Maroto. Modeling of electrokinetic processes by finite element integration of the Nernst-Planck-Poisson system of equations. Sep. Purif. Technol., 79(2):183–192, 2011.
[41] Pulay Peter. Convergence acceleration of iterative sequences. Chem. Phys. Lett., 73(2):393–398, 1980.
[42] C. S. Rafferty, M. R. Pinto, and R. W. Dutton. Iterative methods in semiconductor device simulation. IEEE T. Electron Dev., 32(10):2018–2027, 1985.
[43] W. Rocchia, E. Alexov, and B. Honig. Extending the applicability of the nonlinear Poisson-Boltzmann equation: Multiple dielectric constants and multivalent ions. J. Phys. Chem. B, 105(28):6507–6514, 2001.
[44] B. Roux. Theoretical and computational models of ion channels. Curr. Opin. Struc. Biol., 12(2):182–189, 2002.
[45] Isaak Rubinstein. Electro-diffusion of ions, volume 11. SIAM, 1990.
[46] Y. Saad and Y. Saad. Iterative methods for sparse linear systems, volume 20. PWS publishing company Boston, 1996.
[47] Z. Schuss, B. Nadler, and R.S. Eisenberg. Derivation of Poisson and Nernst-Planck equations in a bath and channel from a molecular model. Phys. Rev. E, 64(3):036116, 2001.
[48] H. Si and A. TetGen. A quality tetrahedral mesh generator and three-dimensional delaunay triangulator. WEIERSTRASS INST FOR APPLIED ANALYSIS AND STOCHASTICS BERLIN (GERMAN), 2006.
[49] Hang Si. Tetview: A tetrahedral mesh and piecewise linear complex viewer. http://tetgen.berlios.de/tetview.html, 2004.
[50] B. F. Smith, P. E. Bjørstad, and W. Gropp. Domain decomposition: parallel multilevel methods for elliptic partial differential equations. Cambridge Univ. Pr., 2004.
[51] Tomasz Sokalski and Andrzej Lewenstam. Application of Nernst-Planck and Poisson equations for interpretation of liquid-junction and membrane potentials in real-time and space domains. Electrochem. Commun., 3(3):107–112, 2001.
[52] A. Zaharescu, E. Boyer, and R. Horaud. Transformesh: A topology-adaptive mesh-based approach to surface evolution. In Proceedings of the 8th Asian conference on Computer vision-Volume Part II, pages 166–175. Springer-Verlag, 2007.
[53] Linbo Zhang. A parallel algorithm for adaptive local refinement of tetrahedral meshes using bisection. Numer. Math. Theor. Meth. Appl., 2(1):65–89, 2009.
[54] Q. Zheng, D. Chen, and G. W. Wei. Second-order Poisson-Nernst-Planck solver for ion transport. J. Comput. Phys., 230(13):5239–5262, 2011.

[55] Konstantin Zhurov, Edmund J.F. Dickinson, and Richard G. Compton. Dynamic simulation of the moving boundary method for measuring transference numbers. Chem. Phys. Lett., 513(1-3):136–138, 2011.